The 12th International Conference on Motion and Vibration
MOVIC2014

Experimental study on harvesting energy from a parametrically excited system

Bahareh ZAGHARI, Emiliano RUSTIGHI and Maryam GHANDCHI-TEHRANI
Institute of Sound and Vibration Research, University of Southampton
Highfield, Southampton, SO17 1BJ, United Kingdom
E-mail: erustighi@soton.ac.uk

Abstract
Vibrations in mechanical structures are usually undesired and dangerous; hence many technologies have been developed in the past to dissipate their mechanical energy. However, it is advisable to harvest such energy, rather than let it dissipate. The harvested vibration energy may be readily used, for example, to independently power sensors due to the small amount of power required to operate them. Numerous linear and non-linear energy harvesters have been proposed in order to operate in a variety of vibratory environments with the intention of improving power production and/or frequency and dynamic range bandwidth of the generic device. In this paper, the suitability of a parametrically excited system versus a non-parametrically excited system for energy harvesting is investigated both numerically and experimentally. Parametrically excited systems show large periodic motion when excited near their region of instability. Firstly, the characteristics of a Single Degree of Freedom (SDOF) system with periodic stiffness are introduced theoretically. A periodic stiffness or parametric stiffness (described by a Mathieu equation) is then introduced into the dynamic equation in order to generate parametric resonance. A cantilever beam with a parametric spring attached along its length is considered. The periodically changing spring coefficient is obtained experimentally using a permanent magnet and two electromagnetic coils as an electromagnetic spring. It is shown that the cantilever beam, when excited parametrically, exhibits the same behaviour described by the Mathieu equation. Numerical and experimental results are in a good agreement.

Keywords : Energy Harvesting, Parametric System, Nonlinear System

1. Introduction

Vibration Energy Harvesting is the transformation of vibration energy present in the environment into electrical energy. In recent years, different vibration-based energy harvesting methods have become a popular research topic, (Ledezma-Ramirez, et al,. 2008), (Zilletti, et al., 2012), (Di Monaco, et al., 2013), (Ghandchi Tehrani and Elliott, 2014). Most of the harvesters are based on a vibrating mechanical structure, usually with additional seismic mass, where the driving force is applied parallel to the direction of the oscillatory displacement (see Fig. 1a). In linear SDOF systems, the maximum displacement occurs at the resonance frequency. Linear harvesters harvest the most energy when the natural frequency of the harvester and environmental frequency match. Consequently, when the response frequency of the energy harvester does not match with the ambient frequency, the output power will decrease. This restricts the development and performance of linear harvesters. In order to solve this problem, different tuning and broadband methods have been proposed (Jang, 2011), but little work has been done in parametric excitation in the context of vibration energy harvesting (Daqaq, et al., 2009).

A physical system that has a periodic time-variant parameter is a system that is parametrically excited. A playground swing-set is a simple example of parametric excitation in a physical system. The swing can be considered as a pendulum whose length changes with time in a periodic manner, in much the same way as the user of the swing will squat to increase their swing height. If the frequency of the periodic oscillation of the swing is equal to twice the frequency of the natural oscillation from the user, the amplitude will increase progressively. Parametric excitation can

only occur in systems with natural oscillations. Furthermore if such a system has a frictional aspect, the amplitude with which the parameter changes (string length in the above example) must exceed a certain threshold. If the aforementioned criteria are achieved, parametric resonance results. Large amplitude cable oscillations caused by parametric excitation due to support, deck or tower motions were observed in cable-stayed bridges (Costa, et al., 1996). This kind of cable oscillation, hereafter referred to as "parametric oscillation of the stay cables", is induced either by motor vehicle traffic, gusts of wind, or a combination of these phenomena. The oscillations of a cable under axial excitation are described by the Mathieu differential equation detailed in Section 2. It is also worth noting that, parametrically excited vibrations can be seen in rotation, such as the roll motion of ships and the vibration of gears (Xie, 2006). Parametric instability analysis of cable stayed bridges has been covered by several researchers such as Siringoringo and Fujino (2012) and Denoël and Degée (2008). Parametric excitation is exploited to increase damping in the system. Another example of parametric system can be seen in Dohnal and Mace (Dohnal and Mace, 2008), where a parametrically excited beam is investigated to determine whether or not damping can be increased. It was found that the effect of coupling modes by parametric excitation leads to additional damping. The parametric excitation is introduced to the cantilever beam by alternating the beam stiffness periodically. The experimental model of Dohnal and Mace for the parametrically excited beam was similar to the one which was introduced by C.C-Chen (2000). Han et.al (2010) carried out the work analytically and experimentally. Alhazza et al. (2008) introduced another application of parametric systems: a non-linear delayed-feedback control on a parametrically excited cantilever beam where the cantilever beam is subjected to a parametric base excitation perpendicular to the oscillatory displacement of the beam.

In terms of energy harvesting, first in 2009, Daqaq et al. investigated the process of energy harvesting via a parametrically excited cantilever beam experimentally and analytically. The cantilever beam was excited vertically, perpendicular to the direction of the oscillatory displacement. In this case, when the beam is excited at twice of its fundamental frequency, parametric resonance can be induced in the cantilever. This establishes an autoparametric resonance (Tondl, 2000). Autoparametric resonance, which is externally induced by parametric resonance, occurs when the resulting vibration of a primary system acts as parametric excitation for the secondary system. This can produce a large system response suitable for energy harvesting. In 2011, Abdelkefi et al. considered the same parametrically excited harvesting beam configuration, but included higher modes and nonlinear effects of the piezoelectric patch in their analysis. In 2013, Jia and Seshia presented an experimental feasibility study on the use of parametrically excited bi-stable systems to increase harvested power. Jia et al. (2013) investigated a parametrically excited MEMS vibration energy harvester numerically and experimentally. They explained the usability of parametric resonance over the fundamental mode, which was not limited by the system damping ratio. They also demonstrated an increase in power density and frequency bandwidth for the parametrically excited MEMS vibration energy harvester.

In this study, we verify, numerically and experimentally, that the harvestable energy is greater in parametric system than in non-parametric systems. First a parametric system is introduced, which is a single degree-of-freedom (SDOF) mechanical oscillator with time-varying stiffness. In order to evaluate the harvestable energy the mass movement will be considered as the displacement of the base of a linear inertial harvester. A cantilever beam with time-varying stiffness is used to produce the parametrically excitated. The experimental setup for the parametrically excited beam is similar to the setup as explained by Dohnal and Mace (2008). In addition, a piezoelectric ceramic patch is used as a generator to convert the mechanical energy to electrical energy.

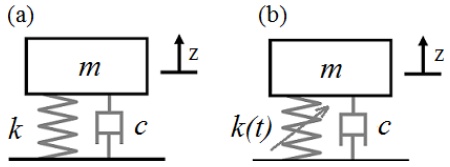

Fig. 1 Single degree-of-freedom system with (a) constant stiffness (non-parametric system), and (b) periodic time-varying stiffness (parametric system).

2. Theory

A SDOF parametric system with time-varying stiffness, as shown in Fig. 1b, is taken into account. The governing differential equation of motion for the parametric system is the generic damped Mathieu equation

$$m\frac{\mathrm{d}^2\mathrm{z(t)}}{\mathrm{dt}^2}+c\frac{\mathrm{dz(t)}}{\mathrm{dt}}+k(t)\,\mathrm{z(t)}=0, \tag{1}$$

where m is the mass, c is the viscous damping coefficient, $\mathrm{z(t)}$ is the mass displacement and $k(t)$ is a time-varying stiffness

$$k(t)=k_c+k_p\cos(\Omega \mathrm{t}), \tag{2}$$

where k_c is the constant stiffness and k_p is the parametric stiffness with the parametric frequency Ω. Since the system is parametrically excited, the harvester does not only respond at the fundamental frequency ω_n, but also at its combined resonances such as $\omega_n \pm \Omega$ (Nayfeh, and Mook, 2008).

Table 1 Properties of the non-parametric and parametric system

	Non-parametric	Parametric
Mass m	0.1 kg	0.1 kg
Viscous damping coefficient c	0.5 $\mathrm{Nsm^{-1}}$	0.5 $\mathrm{Nsm^{-1}}$
Viscous damping coefficient c_{load}	0.056 $\mathrm{Nsm^{-1}}$	0.056 $\mathrm{Nsm^{-1}}$
Constant stiffness k_c	35.4 $\mathrm{Nm^{-1}}$	35.4 $\mathrm{Nm^{-1}}$
Parametric stiffness k_p	-	Varies in different tests

Numerical simulations have been carried out using variable-step fourth-order Runge-Kutta (MATLAB ODE45) to find the time domain response of Eq. (1). Time domain histories and the Fast Fourier Transform of the non-parametric and parametric systems, with parameters given in Table 1 for the case of different parametric frequencies, are obtained. Parameters in table 1 are considered same as the experimental setup properties which is presented in Section 3. Five different tests are carried out in order to look at the behaviour of the non-parametric and parametric system at different parametric stiffness and parametric frequencies. Test1 is corresponding to the non-parametric system and test 2 to 5 are corresponding to the parametric system. Each test is done for a different value of parametric stiffness and frequency for a parametric system and it is presented in Table 2.

Table 2 Free response vibration tests for a non-parametric and a parametric system.

	Test1 Non-parametric	Test2 Parametric	Test3 Parametric	Test4 Parametric	Test5 Parametric-unstable
Parametric stiffness k_p	0	32 $\mathrm{Nm^{-1}}$	15.32 $\mathrm{Nm^{-1}}$	21.32 $\mathrm{Nm^{-1}}$	21.5 $\mathrm{Nm^{-1}}$
Parametric frequency Ω	0	$\Omega=\omega_n$	$\Omega=2\omega_n$	$\Omega=2\omega_n$	$\Omega=2\omega_n$
Average harvested power P	5.06 µW	18 µW	8.8 µW	389 µW	No power

Figure 2. shows the test's results, for the test 1 the time domain response of the non-parametric system (when k_p is equal to zero) with initial conditions $\mathrm{z}(0)=0.01$ m and $\frac{dz}{dt}(0)=0$ at $t=0$. With the presence of damping excitation, the time domain response is damped after 5 seconds of simulation. The frequency response (see Fig. 2(f)) shows that the system resonates at the fundamental frequency $\omega_n=18.82\ \mathrm{Rad\,s^{-1}}$. However, for the parametric system (see Figs. 2(b)-(e)), the parametric frequency and parametric stiffness can change the time domain and frequency response of Eq. (1). In test 2, the parametric stiffness $k_p=32\ \mathrm{Nm^{-1}}$ when the parametric frequency is equal the natural frequency, the time domain results are bounded and shows the system is stable. With the existence of the parametric frequency, the system resonates at the fundamental frequency as well as their combinations. The $\omega_n+\Omega$ frequency can be seen in Fig. 2(h). In test 3, the parametric stiffness $k_p=15.32\ \mathrm{Nm^{-1}}$ when the parametric frequency is twice the natural frequency, the time domain results are bounded and shows the system is stable. The time domain response shown in Fig. 2(c). In test 4, the parametric stiffness $k_p=21.32\ \mathrm{Nm^{-1}}$ when the parametric frequency is twice the natural frequency, the time domain results are bounded and shows the system is stable. The time domain response shown in Fig. 2(d) shows that the parametric system has higher amplitude than the non-parametric system when the parametric frequency is twice the fundamental frequency. The system can be tuned at this frequency within the stable regions, in order to have higher mass displacement and harvest more energy. This can be checked by attaching an accelerometer on top of the mass shown in Fig. 1b. In test 5, when the parametric frequency is twice of the fundamental frequency $\Omega=2\omega_n$ and the parametric stiffness is $k_p=21.5\ \mathrm{Nm^{-1}}$, the time domain response is unbounded. The system with these parameters is unstable. The time domain and frequency domain just for 40 sec of

simulation are shown in Fig. 1(e) and 1(j). In the frequency domain response it can be seen that the magnitude of the response at the fundamental frequencies and combined frequencies is greater when the system is unstable. Also the natural frequency for the parametric system has changed compare to the non-parametric system. The change of the natural frequency is due to the change of the stiffness.

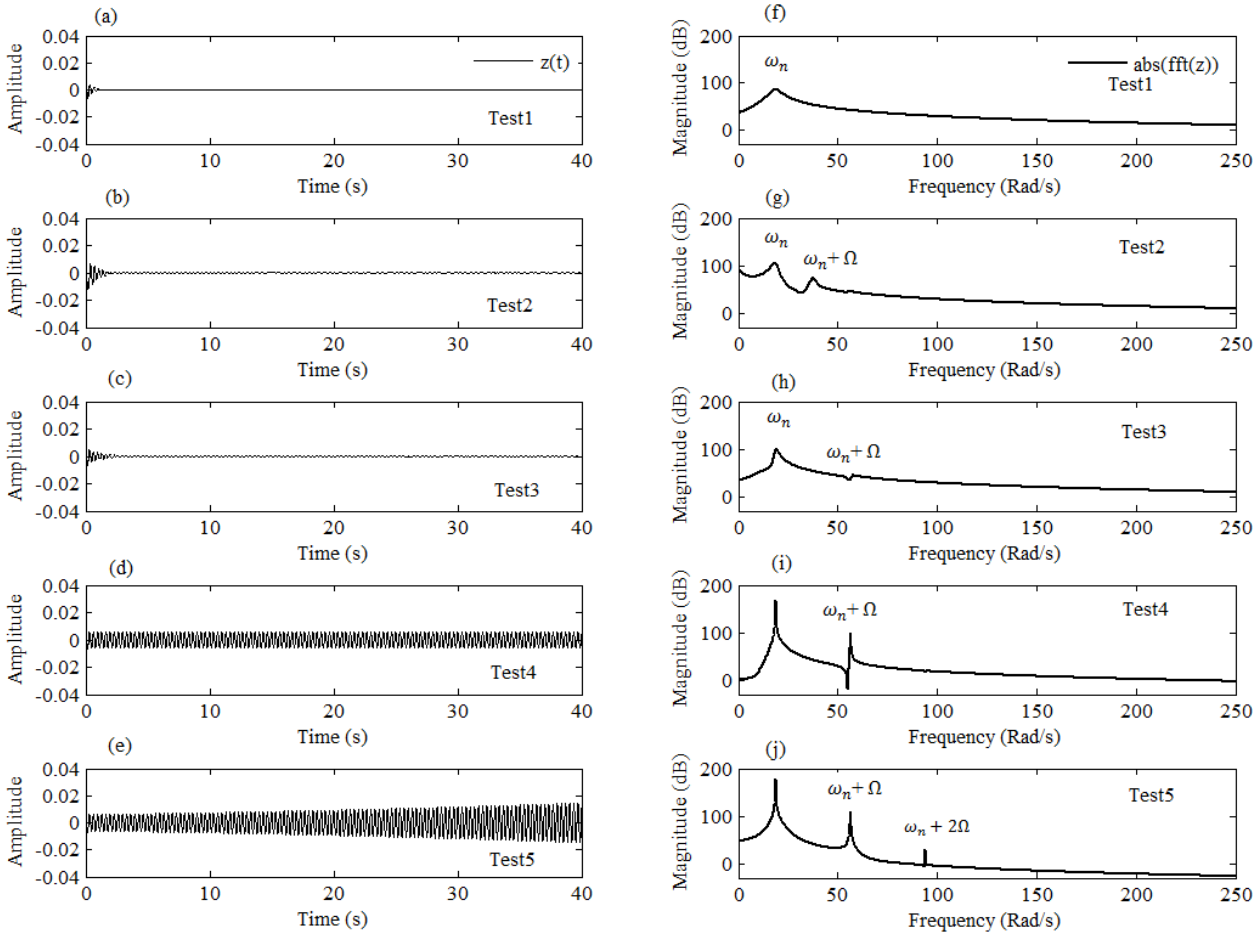

Fig. 2 Numerical solution of non-parametric and parametric SDOF computed with MATLAB ODE45. Time and Frequency response of : a non-parametric system for test1 (a,f), a stable parametric system for test2 (b,g), a stable parametric system for test3 (c,h), a stable parametric system for test4 (d,i), and an unstable parametric system for test4 (e,j).

The power dissipated from a damping load shows the power harvested by the non-parametric and parametric system. The load damping coefficient is coming from the piezoelectric sensor used as a harvester in the experimental setup. The damping load is calculated from the difference between the damping coefficient of the system without the load resistance parallel to the piezoelectric and with the load resistance. The load damping coefficient value is calculated with half-power method and it is shown in Table 1. The power dissipated from a damping load calculated numerically for the non-parametric and parametric system. The average dissipated power for 40 second of free vibration response can be found as

$$P = \frac{1}{T}\int_0^{\mathrm{T}} c_{load}\dot{z}^2 \,\mathrm{dt}. \tag{3}$$

The average dissipated power for five tests explained previously as shown in Table 2 are considered. In test 1, for the non-parametric system the energy is found less than test 2,3 and 4 which are the stable parametric systems. In test 5 as the system is unstable they were no power harvested. By comparison, test 2 and 4 can be seen that test 4 has a higher absorbed power. It shows that when the parametric frequency of the system is tuned at twice of the natural frequency, the average dissipated power is higher.

2.1. A Cantilever Beam Subjected to Electromagnetic Stiffness

In order to verify these results with experimental work, a real system is proposed. A cantilever beam will be subjected to an electromagnetic stiffness emulating the time-variant stiffness in the parametric system. The electromagnetic device consists of a pair of magnets and a pair of coils used to alter the stiffness of the cantilever beam. As shown in Fig. 3 the pair of magnets are fixed to the beam and the pair of coils is fixed to the wood support. The pair of coils has the same number of turns and winding direction. In order to emulate the extra stiffness in the beam, the mutual acting forces between the coils and magnets must cause the electromagnetic device to act like a spring. When the DC current has the direction and the magnets are in the position shown Fig. 3, the mutual acting forces between the magnet and coils are repulsive. This causes the magnets and the attached beam to return to their equilibrium position when displaced. In this case the stiffness produced by the electromagnetic device is positive. If the magnets are reversed an attractive force is generated and negative stiffness is obtained. The negative stiffness comes from the fact that the attractive force pushes the magnet away from equilibrium position. When the coil has an AC current a time-varying stiffness is produced. The time-varying stiffness is proportional to the current through the coil.

In order to predict the behaviour of the electromagnetic system, the magnets and coils are modelled as shown in Fig. 4. The magnetic field produced by the coils and the magnets can be calculated assuming that the coils are perfect and identical solenoids and that the magnets constitute a magnetic dipole. In Fig. 4 the cantilever beam between the two magnets are considered to be at equilibrium when the two coils, traversed by the same current, are positioned at the same distance h from the dipole, and the magnetic field produced by the coils causes no movement along the z axis.

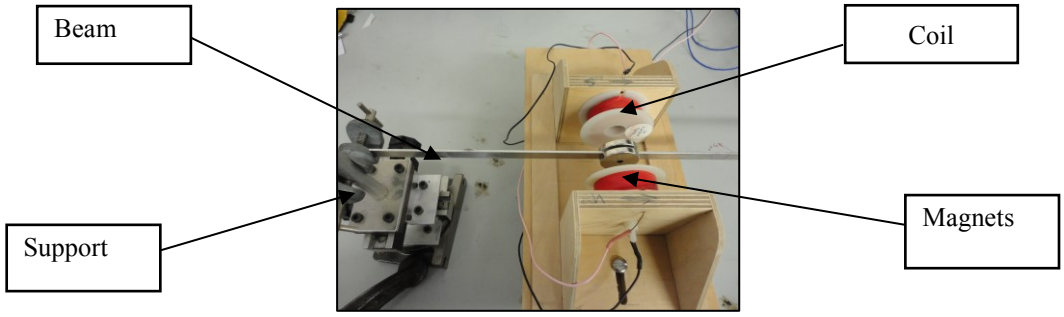

Fig. 3 Schematic of the electromagnetic device, consisting of two coils and two magnets.

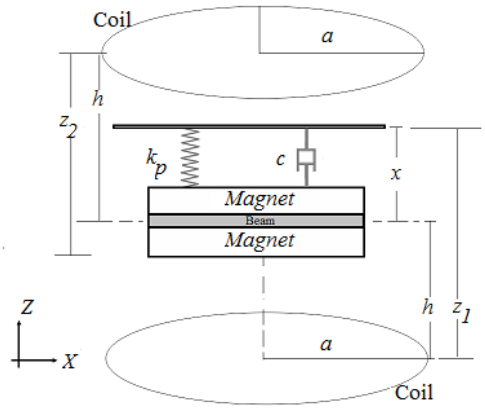

Fig. 4 Coils and magnets configuration.

A SDOF motion equation along the z axis is used to find the motion of the mass between the coils when the coils are in attraction and repulsion. The equation of motion is expressed by

$$m\frac{\mathrm{d}^2 z_1}{\mathrm{d}t^2} + c\frac{\mathrm{d}z_1}{\mathrm{d}t} + k\, z_1 + \mu\frac{\mathrm{d}B_{z_1}}{\mathrm{d}z_1} = 0, \text{ and} \tag{4}$$

$$m\frac{\mathrm{d}^2 z_2}{\mathrm{d}t^2} + c\frac{\mathrm{d}z_2}{\mathrm{d}t} + k\, z_2 + \mu\frac{\mathrm{d}B_{z_2}}{\mathrm{d}z_2} = 0,$$

where the magnetic dipole moment μ is

$$\mu = N\,\pi r^2. \tag{5}$$

where r is the radius of the magnet. Based on Faraday's law, the magnetic field generated by the coil with current I is

$$B_z = \frac{\mu_0 I\,N\,a^2}{2\sqrt{(a^2+z^2)^3}}, \tag{6}$$

where N is the number of turns, μ_0 is the permeability of free space, and a is the coil radius. Therefore the equation of motion can be expressed by Eq. (7) when the system is in repulsion (z_1 and z_2 are in opposite direction)

$$m\frac{\mathrm{d}^2\mathrm{x}}{\mathrm{dt}^2} + c\frac{\mathrm{dx}}{\mathrm{dt}} + k\,\mathrm{x} - G\,\frac{\mathrm{x}+h}{(a^2+(\mathrm{x}+h)^2)^{\frac{5}{2}}} + G\,\frac{\mathrm{x}-h}{(a^2+(\mathrm{x}-h)^2)^{\frac{5}{2}}} = 0 \tag{7}$$

Where G is a constant value

$$G = \frac{3\,\mu\,\mu_0 I\,N\,a^2}{2}. \tag{8}$$

By using the Taylor expansion, Eq. (7) can be expressed as

$$m\frac{\mathrm{d}^2\mathrm{x}}{\mathrm{dt}^2} + c\frac{\mathrm{dx}}{\mathrm{dt}} + k\,\mathrm{x} + k_p\mathrm{x} + k_3\mathrm{x}^3 = 0, \tag{9}$$

where

$$k_p = \left(\frac{-2G}{(a^2+h^2)^{\frac{5}{2}}} + \frac{10Gh^2}{(a^2+h^2)^{\frac{7}{2}}}\right) I = \beta\, I. \tag{10}$$

$k_p = \beta\, I$ is used hereafter for simplicity to show the linear relationship between electromagnetic stiffness and current. The cubic term

$$k_3 = 5\left(\frac{G}{(a^2+h^2)^{\frac{7}{2}}} - \frac{14\,Gh^2}{(a^2+h^2)^{\frac{9}{2}}} + \frac{21\,Gh^4}{(a^2+h^2)^{\frac{11}{2}}}\right), \tag{11}$$

defines the non-linear behaviour of the system. The non-linear terms can be neglected at low current, because the non-linearity reduces with the current. Figure 5 demonstrates this effect, as such, the non-linear term is not considered further.

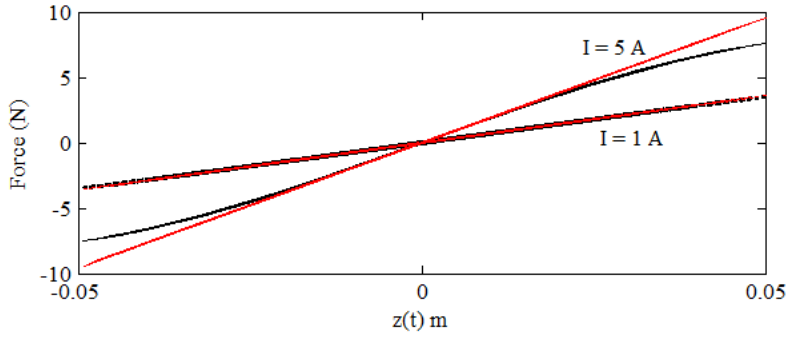

Fig. 5 Two different simulations with different DC currents are simulated. For currents I = 1A and I = 5A, the force at different positions of the cantilever beam is presented. The black lines and red lines show force in the non-linear and linear systems respectively.

2.2. Fundamental Frequencies of a Cantilever Beam Subjected to Parametric Stiffness

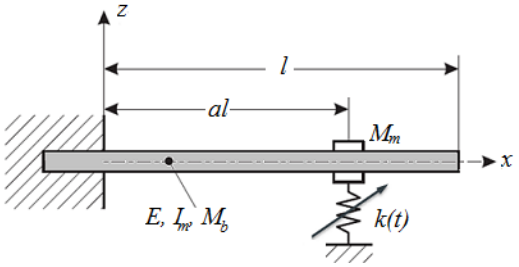

Fig. 6 Cantilever beam with parametric stiffness.

As explained in section 2.1, two coils and two magnets can be used to produce parametric stiffness. A cantilever beam with an electromagnetic device is modelled as a beam carrying a concentrated mass and a parametric stiffness as shown in Fig. 6. The Rayleigh Energy method (Thomson, 1996) is used here in order to find the fundamental frequencies of the system. The cantilever beam with supported spring is assumed to have the mode shape

$$\varphi(x) = \frac{\cos(kl) + \cosh(kl)}{\sin(kl) + \sinh(kl)}(\cos(kx) - \cosh(kx) + \sin(kx) - \sinh(kx)), \tag{12}$$

where $kl = 1.875$, which is the first mode shape of a cantilever beam only. The fundamental frequency when the concentrated mass and stiffness are 0.27 m away from the support ($l = 0.57$ m) is found to be

$$\omega_n = \sqrt{\frac{61.4\, I_m E + k_p R_1}{0.52\, M_b + M_m R_1}} \tag{13}$$

$$R_1 = 0.5\,(-1.36\cos(3.28\,al) + 1.36\cosh(3.28\,al) + \sin(3.28\,al) - \sinh(3.28\,al))^{\,2}, \tag{14}$$

where M_b is the mass of the beam, M_m is the mass of the magnets, E is the Young's modulus, I_m is the moment of inertia, al is the distance of the magnet and coils with respect to the fixing point, and k_p is the electromagnetic stiffness. From Eq. (10) in Section 2.1, the relationship between electromagnetic stiffness and the current flow in the coils is found analytically. So from the relation between fundamental frequency and electromagnetic stiffness, the relation between current flow and fundamental frequency can be found by substituting Eq. (10) to Eq. (13)

$$\omega_n = \sqrt{\frac{61.4\, I_m E + \beta\, I\, R_1}{0.52\, M_b + 0.5\, M_m R_1}} \tag{15}$$

3. Experiment on a Cantilever Beam Subjected to Electromagnetic Stiffness

Figure 7. shows the experimental setup used to generate the periodic electromagnetic stiffness on a cantilever beam. A signal generator and a LAMBDA Zup 10-20 amplifier are used to generate DC and AC current through the coils. A QUATTRO Data Physics DAQ system is used to record data. The beam displacement is measured by a POLYTECH OFV056 laser vibrometer. An aluminium support is used to clamp the cantilever beam in a fixed orientation and location. In order to decrease the vertical movement of the beam, the beam has to be precisely located between the axis of the two coils. This position has been confirmed by entering the attractive mode of the magnets, and returning to the repulsion mode once the centred state is reached. The data in this paper is recorded when the electromagnetic system is in two positions, for position 1 and 2 the electromagnetic system is 0.27 m and 0.37 m away from the support end. The vibrometer is reading at 0.47 m away from the support end. The electromagnetic system and the beam configuration are defined in Tables 3 and 4.

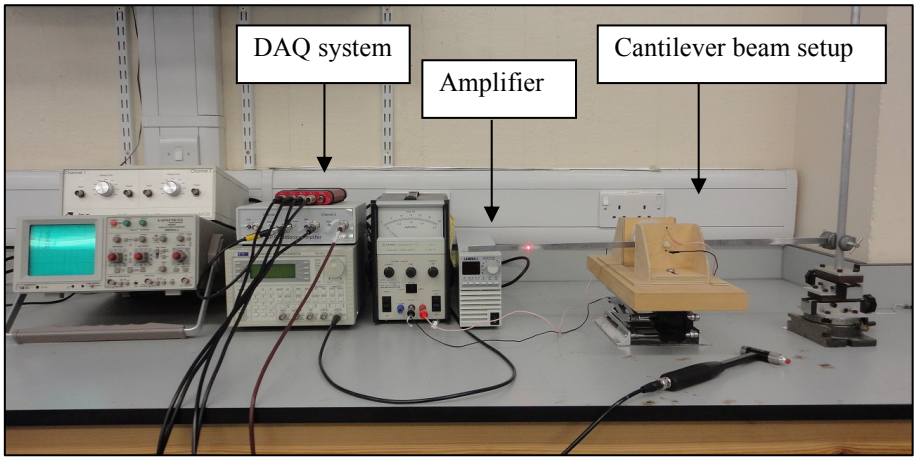

Fig. 7 Experimental setup.

Table 3 Mechanical properties and dimensions of the cantilever beam.

Mechanical properties and dimensions	Value
Material of the beam	Aluminium
Young's modulus E	70×10^9 Pa
Length l	0.57 m
Width b	0.01 m
Thickness d	0.002 m
Mounting position 1 al	0.27 m
Mounting position 2 al	0.37 m
Mounting stiffness k_c at position 1	58.14 Nm^{-1}
Mounting stiffness k_c at position 2	35.4 Nm^{-1}
Beam Mass M_b	0.034 kg

Table 4 Parameters and structural dimensions of the electromagnetic device.

Electromagnetic system and dimensions	Value
Outer radius of permanent magnet	0.015 m
Inner radius of permanent magnet	0.0025 m
Mass of magnets	0.067 kg
Thickness of permanent magnets	0.005 m
Outer radius of permanent coil	0.03 m
Inner radius of permanent coil	0.005 m
Distance between coils	0.04 m
Number of turns in coil	589

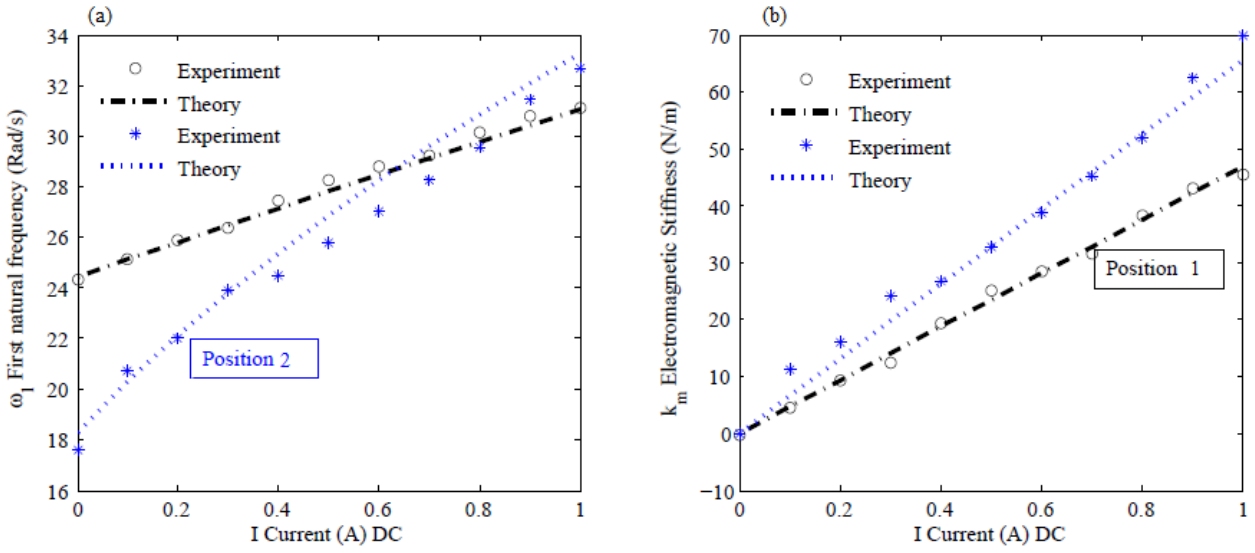

Fig. 8 Comparison between the corrected theoretical and the experimental tested results for DC coil current at position 1 (in black) and 2 (in blue). (a): The variations of first fundamental frequency with DC coil current. (b): The variations of electromagnetic stiffness with DC coil current.

4. Natural Frequencies and Electromagnetic Stiffness of the Cantilever Beam with DC Current Test

In order to find the natural frequencies of the cantilever beam, different DC currents are considered. The electromagnetic system is positioned into position 1 and position 2. An impact hammer with a force transducer is used to excite the beam at both positions. A vibrometer laser is used to measure the dynamic behaviour of the beam.

The DC current that makes the electromagnetic stiffness positive (repulsion mode) is defined to have a positive direction. When the DC current flows through the coils in the impact test, an impulsive excitation is applied to the

cantilever beam by the hammer. A laser is used to read the displacement at the tip of the beam. By analysing the FFT of the placement of the first bending, the natural frequency was acquired. This process was repeated for different DC current in the range $0.1 \leq I \leq 1$. The natural frequency was found from each test, and the first fundamental frequencies are shown in Fig. 8a. Considering Eq. (13), the experimental electromagnetic stiffness was also found. From this, the electromagnetic stiffness can be found from each current value. From the result in section 2.2, the linear relation between the experimental value of electromagnetic stiffness k_P^{Exp} and the result achieved by theory k_P^{Th} for position 1 can be expressed as $k_P^{Exp} = \alpha_1 \, k_P^{Th} = k_p$ where the correction factor is $\alpha_1 = 3$. The variations of electromagnetic stiffness with DC coil current are shown in Fig. 8b. Same approach is done for position 2, the experimental value of electromagnetic stiffness k_P^{Exp} and the result achieved by theory k_P^{Th} can be expressed as $k_P^{Exp} = \alpha_2 \, k_P^{Th} = k_p$ where the correction factor is $\alpha_2 = 4.2$.

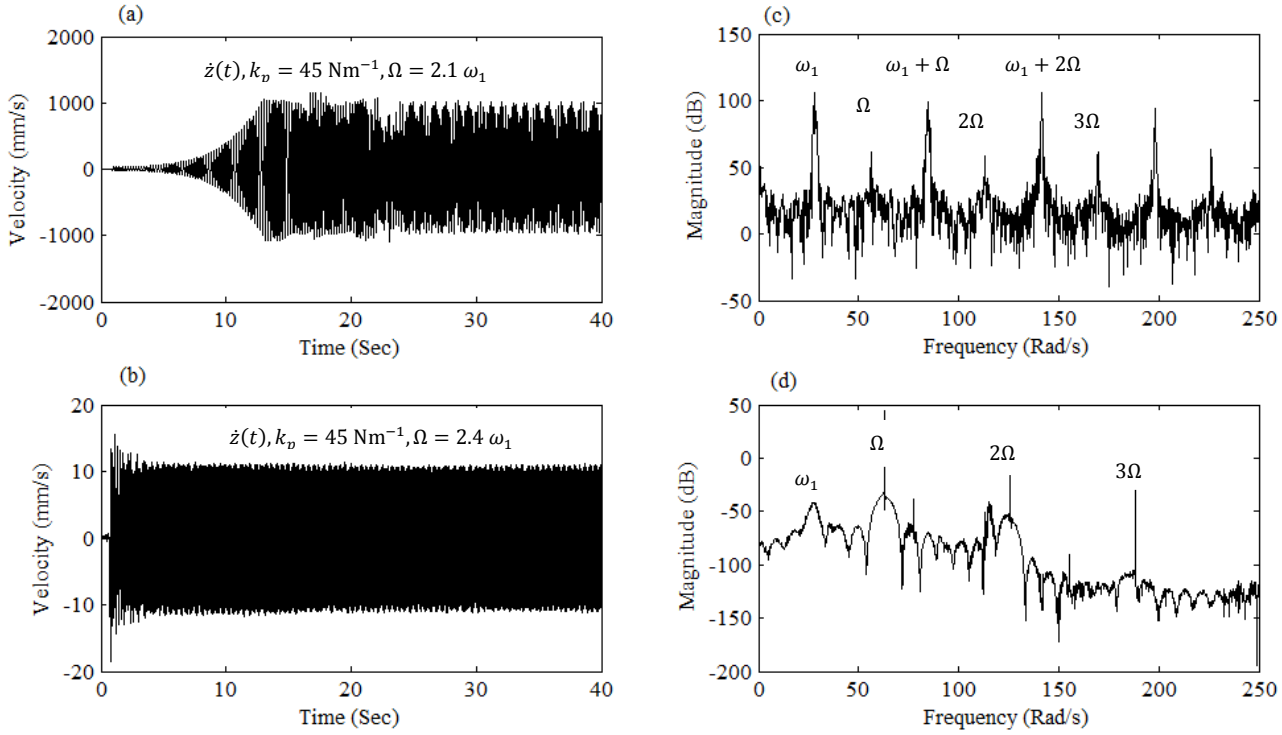

Fig. 9 Time and frequency response behaviour of the parametrically excited cantilever beam from the experimental tests.

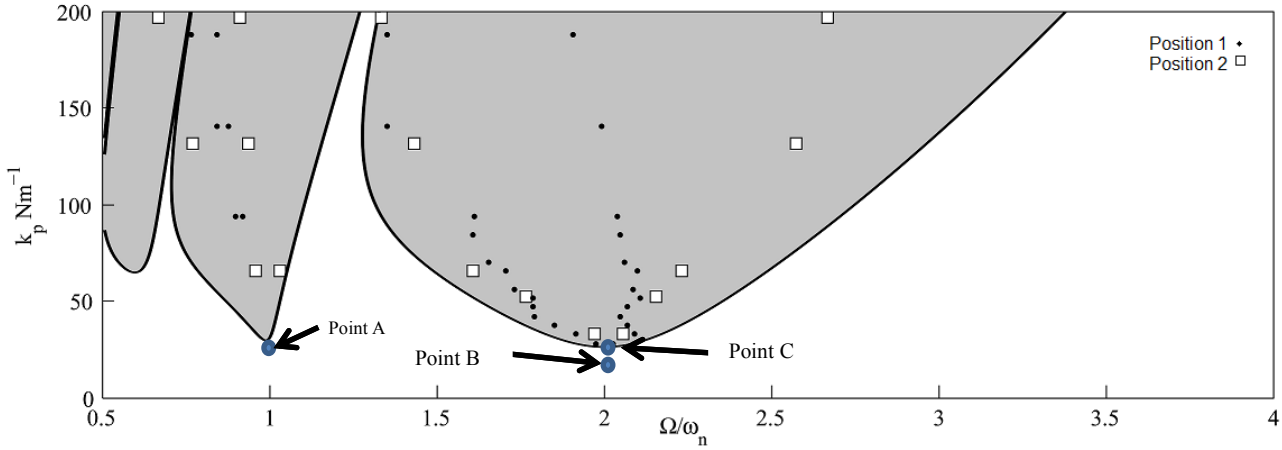

Fig. 10 The experimental and analytical stability plot. Stable and unstable (shaded) area are specified here.

5. Parametrically Excited Cantilever Beam

The AC current flowing through the magnetic device with parametric frequency Ω changes the stiffness of the beam periodically, so the governing equation of the cantilever beam with parametric excitation can be defined as Eq. (1) in Section 2. To test the behaviour of the system, the coil current flow and the velocity of the beam was measured in the lateral axes at different frequencies when the electromagnetic system is placed at position 1 (0.27 m away from the support). Time domain and frequency response for two different parametric frequencies are presented in Fig. 9. When the parametric stiffness is fixed $k_p = 45\text{Nm}^{-1}$, the parametric frequency change, can make the system unstable. In Fig. 9(a) can be seen that the time domain response has increased suddenly in less than 15 sec, which shows the system is unstable. Also looking at the frequency domain shows that the natural frequency and combined frequencies have appeared and they have higher magnitude compare to those in Fig. 9(c). Figure 9(c) shows the frequency response of the stable system. For the stable response when parametric frequency is $\Omega = 2.4\omega_n$ Rad s^{-1} in the frequency domain the natural frequencies and their combined frequencies have lower magnitude and as a result the parametric frequency which comes from the coil currents frequency appears the most. Applying a displacement initial condition or the impact test the other frequencies appear in the frequency response when the system is stable. If these tests carry on for all different value of parametric stiffness and parametric frequency, the stability curves can be plotted. The stability curve shows, the parametric frequency and parametric stiffness change can change the stability of the system. This plot is known as Mathieu stability plot. Analytical stability curve is plotted here based on Harmonic Balanced Method. The analytical stability plot is shown in Fig. 10. The shaded area is the unstable area. The experimental stability curve which is examined by considering different value of parametric stiffness and parametric frequency is plotted in a same graph as analytical stability graph, Fig. 10. The experimental results for position 1 were not matched with the analytical solution so the position 2 is checked for the stability plot. The electromagnetic system is placed at position 2 (0.37 m away from the support).

For different value of parametric stiffness and parametric frequency and different natural frequency (Fig. 8(a)), the stability curve is plotted in Fig. 10. The stability curve when the electromagnetic system is position 2 has a good agreement with analytical solution. Although at lower frequency when the parametric frequency is less than the natural frequency, the analytical solution shows the system is unstable, in experiment system was stable. This might be due to the setup configuration and higher damping in experiment than theory. Also, they are some nonlinearity in the experimental system which has not considered here. The theory here is considered for a Single DOF system and experimental results are based on Two DOF cantilever beam. In order to match the theoretical and experimental data, the experiment which is closer to the Single DOF system has a better match with the theory. This can be seen by choosing position 2, as the electromagnetic system is getting furthered from the support, the first and second natural frequencies are getting away from each other. Then the experiment can be modelled as SDOF system.

6. Energy harvesting from a Parametrically Excited Cantilever Beam

Near the fixed end a piezoelectric sensor is attached to the beam (Fig. (10)). Piezoelectric is a PZT ceramics from PI (Model PIC255). The output voltage from the piezoelectric is measured in open circuit with the using an amplifier with 0dB gain to minimize the piezoelectric impedance to connect to a DAQ system (QUATTRO Data Physics) which has 100mohm output impedance.

Table 5 PZT properties.

Mechanical properties and dimensions	Value
Length l	0.03 m
Width b	0.01 m
Thickness d	0.0005 m

For the purpose of energy harvesting a piezoelectric patch is attached to the beam and connected to a resistive load. A resistive load is considered $R = 10$ kOhm for a comparison of trends for a non-parametric and parametric system at different parametric stiffness and frequency and it has not optimised for the system. In order to find the feasibility of energy harvesting with parametrically excited system, four tests are carried out. First test is done for a non-parametric

system. The second test is for a parametric system, at stable region of the stability curve when the parametric stiffness $k_p = 32\ \mathrm{Nm}^{-1}$ and parametric frequency is equal to the natural frequency $\Omega = \omega_n$ (Point A in Fig. 10). Since the system is stable and damped the piezoelectric output is decayed. Figure 11 shows the piezoelectric output.

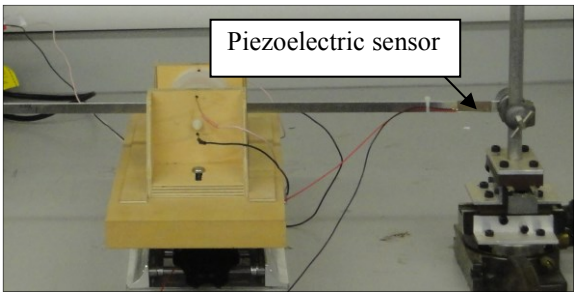

Fig. 10 Piezoelectric actuator on the parametrically excited cantilever beam is fixed close to the support.

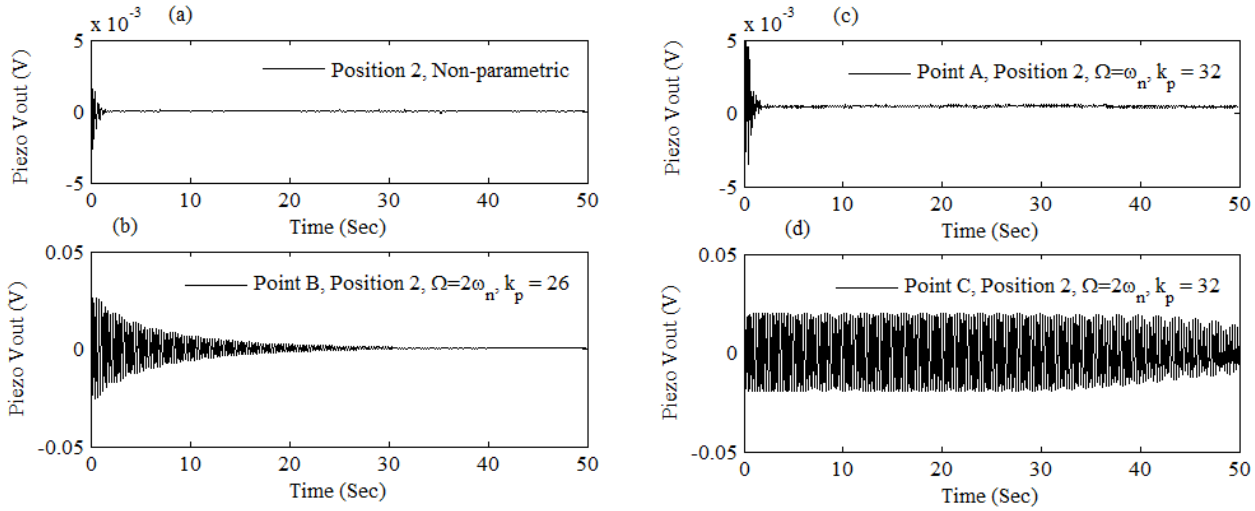

Fig. 11 Piezoelectric voltage output with the load resistance $R = 10$ kOhm.

Table 6 Free response energy for two experimental tests.

	Test1 Non-parametric	Test2 Point A	Test3 Point B	Test4 Point C
Parametric stiffness k_p	-	$32\ \mathrm{Nm}^{-1}$	$26\ \mathrm{Nm}^{-1}$	$32\ \mathrm{Nm}^{-1}$
Parametric frequency Ω	-	$\Omega = \omega_n$	$\Omega = 2\omega_n$	$\Omega = 2\omega_n$
Average harvested power P	0.05 nW	0.5 nW	0.003 μW	0.023 μW

The third test is when the parametric stiffness $k_p = 26\ \mathrm{Nm}^{-1}$ and parametric frequency is twice of the natural frequency $\Omega = 2\omega_n$ (Point B in Fig. 10). Forth test is done close to unstable region when the parametric stiffness $k_p = 32\ \mathrm{Nm}^{-1}$ and parametric frequency is twice of the natural frequency $\Omega = 2\omega_n$ (Point C in Fig. 10). At this point since the system is close to unstable region and it is less damped, the piezoelectric output has not changed within 40 sec. This can be an option for tuning the harvester in order to absorb more power. At Point A and Point B, the power dissipated in the resistor is calculated as

$$P = \frac{1}{T}\int_0^T \frac{1}{R_{load}} V_{piezo}{}^2 \,\mathrm{dt}. \tag{16}$$

The average harvested power is calculated for 40 second measurement for four different tests and shown in Table 6. From Table 6, it can be seen that at point C highest power is harvested. It shows that when the parametric frequency of the system is tuned at twice of the natural frequency and the system is tuned close to the instability region, the power is higher. This comparison is also matches with the numerical dissipated power in section 2 and presented in Table 2.

7. Conclusion

Dynamic characteristic of a linear parametrically excited system is studied numerically and experimentally. An electromagnetic system is used to generate a periodic stiffness on a cantilever beam. Numerically characteristic of non-parametric and parametric system is discussed and the result compared with the experimental results which come from the parametric cantilever beam. The stability curve from the experimental results at two position of the electromagnetic system is considered and compared with the analytical results. In order to get a better experimental stability curve, the electromagnetic system could be position furthered from the support. Other positions with different cantilever beam configuration will be checked as a future work. As a result that the cantilever beam can behave parametrically, the piezoelectric sensor has placed in order to harvest energy. The experimental result from the piezoelectric output shows that there is a possibility to harvest more power when the system is tuned at twice of the natural frequency and the system is tuned close to the instability region.

Acknowledgement

Dr Ghandchi Tehrani would like to acknowledge EPSRC for her first grant (Ref: EP/K005456/1).

References

Abdelkefi, A., A. Nayfeh and M. Hajj, Global nonlinear distributed-parameter model of parametrically excited piezoelectric energy harvesters, Nonlinear Dynamics (2012), 67(2): 1147-1160.

Alhazza, K. A., Daqaq, M. F., Nayfeh, A. H., & Inman, D. J., Non-linear vibrations of parametrically excited cantilever beams subjected to non-linear delayed-feedback control, International Journal of Non-Linear Mechanics (2008), 43(8), 801-812.

Chen, C.-C. and M.-K. Yeh, Parametric instability of a beam under electromagnetic excitation, Journal of sound and vibration (2001), 240(4): 747-764.

Costa, A. P. d., J. Martins, F. Branco and J.-L. Lilien, Oscillations of bridge stay cables induced by periodic motions of deck and/or towers, Journal of Engineering Mechanics (1996), 122(7): 613-622.

Daqaq, M. F., C. Stabler, Y. Qaroush and T. Seuaciuc-Osório, Investigation of power harvesting via parametric excitations, Journal of Intelligent Material Systems and Structures (2009), 20(5): 545-557.

Denoël, V. and H. Degée, Comparison of parametric excitation and excitation of an elastic stay cable, Proceedings of the 7th European Conference on Structural Dynamics (2008).

Di Monaco, F., M. Ghandchi Tehrani, S. J. Elliott, E. Bonisoli and S. Tornincasa, Energy harvesting using semi-active control, Journal of Sound and Vibration (2013), 332(23): 6033-6043.

Dohnal, F. and B. Mace, Amplification of damping of a cantilever beam by parametric excitation, (2008).

Ghandchi Tehrani, M. and S. J. Elliott, Extending the dynamic range of an energy harvester using nonlinear damping, Journal of Sound and Vibration (2014) 333(3): 623-629.

Han, Q., Wang, J., Li, Q., Experimental study on dynamic characteristics of linear parametrically excited system, Mechanical Systems and Signal Processing, (2011) 25(5), 1585-1597.

Jang, S.-J., E. Rustighi, M. Brennan, Y. Lee and H.-J. Jung, Design of a 2DOF vibrational energy harvesting device, Journal of Intelligent Material Systems and Structures (2011) 22(5): 443-448.

Jia, Y. and A. A. Seshia, Directly and parametrically excited bi-stable vibration energy harvester for broadband operation, Solid-State Sensors, Actuators and Microsystems (2013).

Jia, Y., J. Yan, K. Soga and A. A. Seshia, Parametrically excited MEMS vibration energy harvesters with design approaches to overcome the initiation threshold amplitude, Journal of Micromechanics and Microengineering (2013), 23(11): 114007.

Jia, Y., J. Yan, K. Soga and A. A. Seshia, A parametrically excited vibration energy harvester, Journal of Intelligent Material Systems and Structures (2013).

Ledezma-Ramirez, D., N. Ferguson and M. Brennan, Energy dissipation using variable stiffness in a single-degree-of-freedom model (2008).

Nayfeh, A. H. and D. T. Mook Nonlinear oscillations, Wiley. com (2008).

Siringoringo, D. M. and Y. Fujino, Estimating Bridge Fundamental Frequency from Vibration Response of Instrumented Passing Vehicle: Analytical and Experimental Study, Advances in Structural Engineering (2012), 15(3): 417-434.

Thomson, W, Theory of vibration with applications. CRC Press (1996).

Tondl, A., Autoparametric resonance in mechanical systems, Cambridge University Press (2000).

Xie, W.-C., Dynamic stability of structures, Cambridge University Press (2006).

Zilletti, M., S. J. Elliott and E. Rustighi, Optimisation of dynamic vibration absorbers to minimise kinetic energy and maximise internal power dissipation, Journal of Sound and Vibration (2012), 331(18): 4093-4100.